VNU Journal of Science: Mathematics - Physics

Journal homepage: https://js.vnu.edu.vn/MaP

Original Article

Facile Synthesis of g-C_3N_4 for Efficient Photocatalytic Degradation of Rhodamine B

Nguyen Dac Dien[1], Vu Xuan Hoa[2,*], Pham Thi Thu Ha[2], Tran Thu Trang[2], Lai Tong Anh Kiet[2], Vibhawari Dhoble[2], Nguyen Duc Toan[3], Tran Thi Huong Giang[4], Nguyen Thi Luyen[2], Pham Van Hai[5], Pham Thi Nga[2]

[1]*Vietnam Trade Union University, 169 Tay Son, Kim Lien, Hanoi, Vietnam*

[2]*TNU-University of Sciences, Phan Dinh Phung, Thai Nguyen, Vietnam*

[3]*Institute of Materials Science, Vietnam Academy of Science and Technology, 18 Hoang Quoc Viet, Nghia Do, Hanoi, Vietnam*

[4]*Institute of Physics, Vietnam Academy of Science and Technology, 10 Dao Tan, Ngoc Ha, Hanoi, Vietnam*

[5]*Hanoi National University of Education, 136 Xuan Thuy, Cau Giay, Hanoi, Vietnam*

Received 11th June 2026
Revised 15th July 2026; Accepted 31st July 2026

Abstract: Water pollution caused by Rhodamine B (RhB) underscores the need for efficient photocatalytic degradation methods. In this study, g-C_3N_4 nanosheets were synthesized via a one-pot thermal polymerization method, with a constant melamine amount and varying NH_4Cl content. The obtained g-C_3N_4 nanosheets exhibited the lateral size of around 0.5 × 2.5 µm and the thickness of about 6-8 nm. g-C_3N_4 catalysts exhibited high efficiency in the degradation of RhB under ultraviolet (UV) irradiation (365 nm). Within 60 min, RhB degradation reached ~ 99.78% with a rate constant (k) ~ 0.114 min^{-1}. Based on the analytical results, a possible mechanism of photocatalytic degradation was proposed. Its superior performance stems from its numerous active sites and improved surface area, which promoted charge transfer and enhanced redox species generation. Superoxide ($\cdot O_2^-$) and hydroxyl ($\cdot OH$) radicals are the effective agents for photodegrading RhB. This work demonstrates that g-C_3N_4 nanosheets function as an efficient photocatalyst for removing organic pollutants from wastewater.

Keywords: g-C_3N_4, RhB, photocatalyst, UV irradiation.

* Corresponding author.
E-mail address: hoavx@tnus.edu.vn

https//doi.org/10.25073/2588-1124/vnumap.5161

1. Introduction

The escalating problem of global environmental pollution, especially water contamination, is widely regarded as one of the most significant concerns for modern society as it poses a serious threat to terrestrial and marine ecosystems, including human beings [1]. Rapid industrialization has led to increased release of hazardous pollutants such as dyes, insecticides, pesticides, etc. from industrial, agricultural, and livestock farming into wastewater, many of which are toxic, persistent, and difficult to degrade [2].

Colored pigments are broadly utilized across several industries, such as food, leather, printing, paper, fiber, textiles, etc. that discharge a large volume of wastewater containing hazardous substances and organic dyes [3]. The untreated industrial effluents contaminate water bodies like rivers and ponds and raise a major interest for governments and the scientific community. Thus, decontaminating the wastewater would protect the environment and public health as well as the sustainable development of countries.

Organic dyes are categorized into three distinct types: cationic, anionic, and non-ionic. Rhodamine B (RhB) is a cationic dye with positive charge and a chemical formula of $C_{28}H_{31}ClN_2O_3$ [4]. Its chemical structure is illustrated in Figure 1. Due to its intricate aromatic structure, RhB is classified as a secondary diazo dye. It is resistant to biodegradation and rather durable. It is commonly used to determine the direction and velocity of flow thanks to its fluorescent characteristic, and therefore can be easily detected by fluoroscopy. It is also used in biology to detect organisms, especially bacteria, biological macromolecules, and heavy metal ions. In the industrial sector, RhB is a synthetic dye for textiles, clothing, and food.

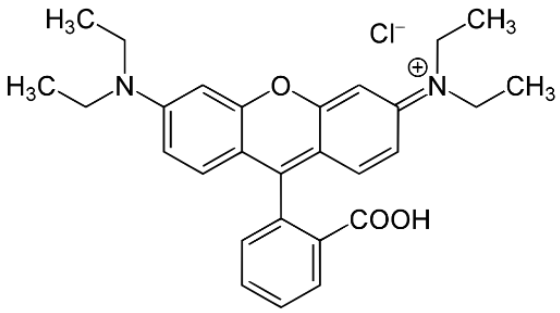

Figure 1. Chemical structure of Rhodamine B (RhB) molecule.

However, it presents a particular concern due to its pronounced biological toxicity, high solubility, and stability in water, which poses challenges in removing it from contaminated water. It exhibits a carcinogenic potential, so products containing it must be labeled with a warning. Exposure to RhB can lead to severe health impacts, such as respiratory damage, tissue necrosis, thus posing a substantial risk to aquatic life and water quality [5]. Therefore, developing effective and sustainable strategies for the removal of RhB is crucial.

Several methods have been applied for RhB removal, consisting of membrane filtration, adsorption, sedimentation, flocculation, reverse osmosis, ozonation, sonophotocatalysis, chemical precipitation, advanced oxidation processes (AOPs), electrochemical processes, biodegradation, flotation, etc. While they are highly effective, their high-cost limits scalability. Photocatalysis has recently gained considerable attention owing to its significant potential in degrading a broad range of organic contaminants. Photocatalytic degradation offers a more economical and greener alternative through the usage of highly active oxidants without causing secondary pollution [6]. Photocatalysts can break down

dyes into harmless products like CO_2 and H_2O under light illumination [7]. Photocatalysts use photoexcited electron-hole pairs over semiconductors to form oxidative radicals to degrade the organic pollutants. The efficiency of photocatalytic reaction strongly depends on various factors, including the surface area, bandgap energy, crystallinity, morphology, composition of catalysts, light wavelength and intensity, the presence of scavengers, pollutant concentration, pH value in the media, and so on.

Graphitic carbon nitride (g-C_3N_4) is one of the eco-friendly and efficient photocatalyst that can degrade RhB into less harmful compounds. g-C_3N_4 is a promising support owing to its stability, ease of synthesis, inexpensive, non-toxic, and semiconducting properties. It shows strong ultraviolet light activity due to its suitable bandgap (2.7 eV) [8], increased surface-active edge sites, effective charge transfer, and high structural porosity. Under UV irradiation, g-C_3N_4 efficiently generates electron-hole pairs enhancing redox capability. Photoinduced electrons produce superoxide radicals ($\cdot O_2^-$), while photogenerated holes produce hydroxyl radicals ($\cdot OH$) [7]. These reactive species mineralize RhB into CO_2, H_2O, and other by-products. g-C_3N_4 is a metal-free polymeric carbon nanomaterial that has received the great interest of researchers. For example, Luu H. Q. et al. have prepared TiO_2@g-C_3N_4 Z-scheme structure to degrade NO in visible light through plasma-treated photocatalytic [9]. Chu C. et al., have synthesized 2D carbon nitride with Co single atom for photocatalytic H_2O_2 production [10]. Zhu Q. et al., modified carbon-based heterostructures by binary heteroatom dopants (S and N) for photocatalytic production of H_2O_2 [11]. Liu B. et al., obtained S-doped g-C_3N_4/$CuFeO_2$ S-scheme heterojunction for photocatalytic removal of RhB with 92.6% efficiency within 3 h [5]. Wang Y. et al., synthesized Pt/g-C_3N_4 heterojunctions via photoreduction by integrating plasma Pt with g-C_3N_4 nanotubes for methyl orange (MO) degradation [12]. Molaei P. et al. synthesized Se/g-C_3N_4 S-scheme heterojunctions through a rapid thermal shock (RTS) strategy for methylene blue (MB) degradation [6]. Yaqoubi M. et al. have fabricated S-scheme $CuMn_2O_4$/g-C_3N_4 heterojunction via a simple two-step technique to destroy erythrosine below visible lamp [13]. Niknam M. et al. have synthesized g-C_3N_4/NiAl-LDH/CeO_2 nanocomposites via a straightforward hydrothermal method for degradation of RhB with an efficiency of 98% under UV irradiation after 350 min [14]. Alekseeva O.V. et al. synthesized TiO_2/g-C_3N_4 composites using sol-gel method for destruction of organic dyes (Rhodamine B, Methylene blue, Reactive Red 6C) under UV light [15]. Almotiry S. et al. prepared BaZnO/g-C_3N_4 nanocomposites for anionic and cationic dyes (Basic fuchsin and Congo red) degradation [8]. Ammar S.H. et al. fabricated S/g-C_3N_4 composites for MB degradation with efficiency of 94.6% within 60 min of visible light [16], and so on. These authors have focused on overcoming issues with single composition catalysts such as limited responsiveness to visible light and rapid charge-carrier recombination. The photocatalytic performance has been improved through surface modification, doping, or heterojunction creation with other semiconductors to suppress electron-hole pair recombination, reduce the bandgap, so enhance visible light absorption and photocatalytic efficiency. To our best knowledge, there are no reports addressing the photocatalytic degradation of RhB dye with individual g-C_3N_4 nanosheets. They offer outstanding benefits such as a large specific surface area, reduced charge-diffusion distance, small bandgap, remarkable redox capacity, straightforward synthesis and can operate as a highly efficient photocatalyst when exposed to UV light [17].

In this work, g-C_3N_4 was developed to address the distinct environmental pollutant (RhB) via photocatalytic degradation. Its superior photocatalytic performance is attributed to its improved charge carrier generation under UV irradiation and reactive species formation. The primary aim of this research is to construct g-C_3N_4 nanosheets photocatalysts and evaluate their photocatalytic effectiveness in the degradation of RhB dye as a model of organic contaminant under UV light.

2. Experimental

2.1. Synthesis Procedure of g-C_3N_4

g-C_3N_4 was prepared via a one-step thermal condensation method employing melamine ($C_3H_6N_6$) and ammonium chloride (NH_4Cl) as precursors. 3 g of melamine and a certain amount of NH_4Cl were ground thoroughly in an agate mortar to achieve uniform mixing. The mixed precursor was dispersed in 10 ml of absolute ethanol (C_2H_5OH). The blended mixture was then placed in a lidded ceramic crucible and subjected to thermal treatment at 520°C for 2 h with a ramp rate of 1°C/min. During the thermal process, melamine underwent decomposition and polymerization, resulting in the formation of graphitic carbon nitride (g-C_3N_4) as following:

$$C_3H_6N_6 \rightarrow C_3N_4 + 2NH_3 \quad (1)$$

Table 1. Amounts of precursors and designation of g-C_3N_4 products

No.	Sample	Melamine (g)	NH_4Cl (g)	Melamine/NH_4Cl ratio
1	g-C_3N_4 6:1	3	0.5	6:1
2	g-C_3N_4 6:2	3	1	6:2
3	g-C_3N_4 6:3	3	1.5	6:3
4	g-C_3N_4 6:4	3	2	6:4
5	g-C_3N_4 6:6	3	3	6:6
6	g-C_3N_4 6:8	3	4	6:8

Simultaneously, ammonia (NH_3) gas was released. After naturally cooling, the dark-coloured powder product was thoroughly washed with ethanol to eliminate residual impurities and dried at 60°C overnight. To investigate the effect of melamine/NH_4Cl ratio on photocatalytic performance of g-C_3N_4, a series of g-C_3N_4 was prepared by varying the amount of NH_4Cl precursor from 0.5 g to 4 g, and the resulting samples were designated as Table 1.

2.2. Characterization

Phase identification and the crystalline nature of g-C_3N_4 were examined using power X-ray diffraction (XRD, Bruker D8 Advance, Germany) with Cu-K_α radiation (0.15418 nm) at 40 kV and a scan rate of 10°/min in the range of 5-65°. The surface morphology was recorded using transmission electron microscopy (TEM, JEOL JEM 1010, Japan) operating at 80 kV. The lattice distance was determined by high resolution transmission electron microscopy (HRTEM, JEOL JEM 1010, Japan) operating at 200 kV. The ultraviolet-visible (UV-Vis) absorption spectra were obtained on a JASCO V770 spectrophotometer (Japan) in the wavelength range of 200-1000 nm. A photoluminescence spectrometer (FLS1000, Scotland) was employed for the photoluminescent spectrum analysis using the exciting wavelength of 365 nm. Energy-dispersive X-ray spectroscopy (EDS) measurement was conducted using Hitachi SU 8020 (Japan).

2.3. Evaluation of Photocatalytic Activity in Rhodamine B Degradation

The precision of the experimental condition was a key factor in ensuring the validity of the results. The photocatalytic efficiency of g-C_3N_4 was investigated by the degradation of RhB in the presence of g-C_3N_4 under UV irradiation at room temperature. In the conventional photocatalytic procedure, six pink solutions of RhB with known concentration of 15 ppm were prepared by dissolving 0.15 mg of RhB in 10 ml of deionized water. Subsequently, 10 mg of g-C_3N_4 was dispersed in each RhB solution, and the mixture was stirred in the dark for 1 h to ensure uniform distribution of the photocatalytic agent as well

as adsorption-desorption equilibrium. The photoreactor comprised a glass beaker fitted with a cooling to maintain the solution temperature at approximately 25°C during the photocatalytic process. 1 ml of the combined solution was taken out to determine the initial dye concentration (C_o) and the remaining mixture was then subjected to UV irradiation (365 nm) from a mercury lamp at the illumination intensity of 1 mW/cm^2. Subsequently, at regular intervals of 10 min, 1 ml of the suspension was withdrawn and analyzed using UV-Vis spectrophotometer within the spectral range of 450-650 nm to evaluate its photodegradation. The photodegradation efficiency of RhB was assessed by measuring the variation in dye concentration through absorbance measurement at λ_{max} = 553 nm using equation (2):

$$E = 1 - \frac{C}{C_o} = 1 - \frac{A}{A_o} \quad (2)$$

where C represents a concentration of dye at irradiation time (t), and C_o denotes the initial concentration of dye, A signifies absorbance at regular intervals, and A_o is the initial absorbance. The pseudo-first-order rate constant value (k) was estimated by linear fitting of $\ln(C_o/C)$ against time plot [18]:

$$\ln(C_o / C) = kt + a \quad (3)$$

3. Results and Discussion

3.1. Characterization

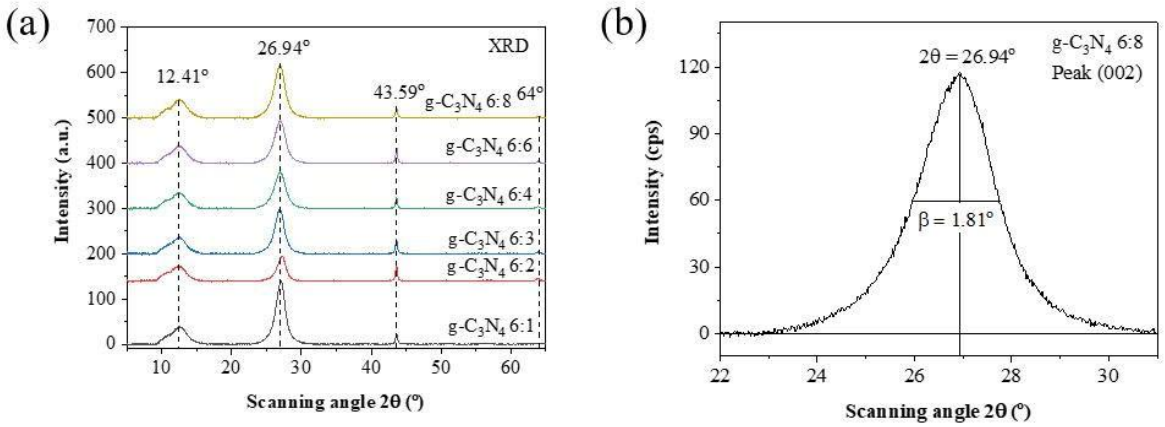

Figure 2. (a) XRD patterns of g-C_3N_4 nanosheets prepared from different melamine/NH_4Cl weight ratios, (b) the crystallite size calculated from the width and position of (002) peak using Debye-Scherrer equation.

Powder XRD pattern was employed to examine the crystal structure, phase component, and purity of the synthesized nanosheets. The diffraction profile was compared with standard reference pattern to confirm the structural phase present. Figure 2a exhibits two distinct diffraction peaks at 2θ value of 26.94° and 12.41°, corresponding to the (002) and (100) planes, respectively. These peaks align accurately with the reference data for g-C_3N_4 (JCPDS No. 087-1526) [19]. The diffraction peaks appear as sharp reflections of graphitic material. The weak (101) diffraction peak at 2θ = 43.59° is due to the axis of the graphite structure, consistent with prior research [20]. The diffraction peak at 64° is very weak and disappeared as a large amount of NH_4Cl was added. These results confirmed the successful formation of g-C_3N_4 phase [21]. The crystallite size is calculated using the Debye-Scherrer equation [22]:

$$D = \frac{k\lambda}{\beta \cos\theta} \quad (4)$$

where D is the crystallite size (nm), λ is the wavelength of X-ray used in the X-ray diffraction experiment, $k = 0.893$ is Scherrer constant, β is the full width at half maximum (FWHM) of the diffraction peak (rad), θ is the Bragg diffraction angle (°). From the calculation result (Figure 2b), the average crystallite size of g-C_3N_4 nanosheets was 4.536 nm.

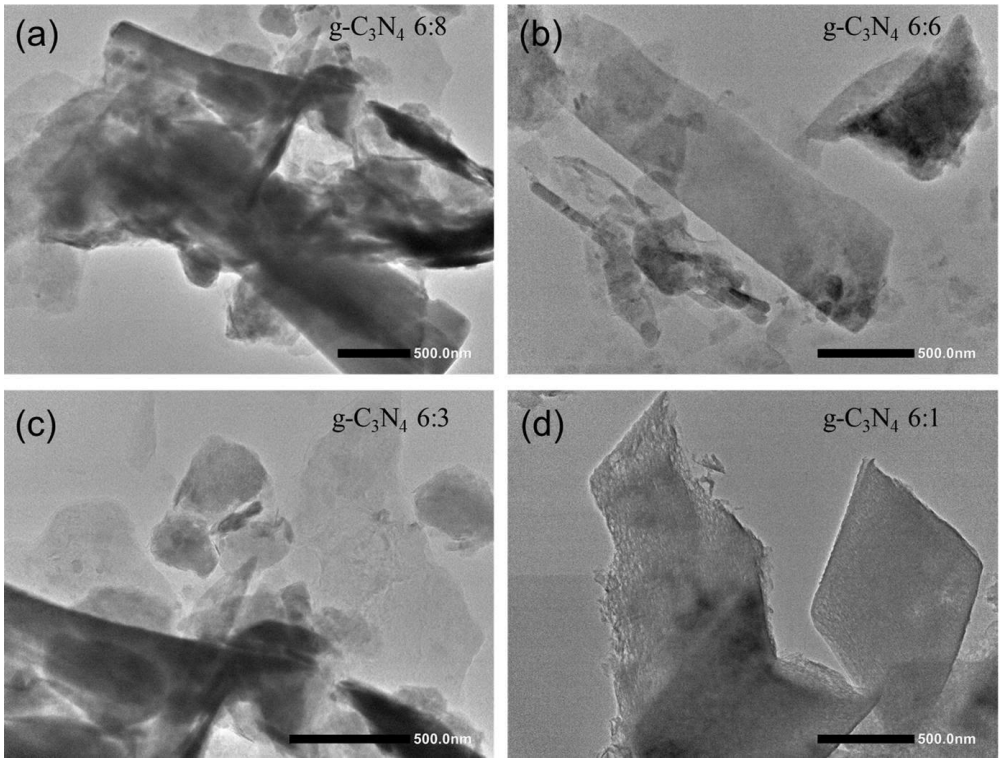

Figure 3. TEM images of g-C_3N_4 nanosheets.

Transmission electron microscopy (TEM) image was performed to study the morphology of g-C_3N_4 with various melamine/NH_4Cl weight ratios (6:8, 6:6, 6:3, and 6:1). Figure 3 provides a clear and visual confirmation of g-C_3N_4 shape with lateral size of 0.5 × 2.5 μm. The g-C_3N_4 sample presents a nanosheet structure and layered nature with a smooth surface, compact arrangement, and thickness ranging from 6 to 8 nm. The stacking structure is highly porous with abundant surface-active sites for dye adsorption, potentially resulting in improved degradation efficiency. These nanosheets form an interconnected network which facilitate efficient charge carrier transport, thereby optimizing the photodegradation process. The structural feature of g-C_3N_4 nanosheets was further elucidated using high-resolution transmission electron microscopy (HRTEM) technique. Figure 4a shows well-defined lattice fringes that are the parallel lines dividing the crystal surfaces, and interplanar d-spacing of 0.323 nm, corresponding to the (002) plane. This result confirms the crystalline nature of g-C_3N_4 nanosheets.

Moreover, photoluminescence (PL) spectra in the range of 380-750 nm were employed to assess the photoluminescent property of materials. The efficacy of photogenerated phenomenon when excited by 365 nm UV, electron-hole recombination rate, and the charge mobility of g-C_3N_4 nanosheets were deduced from Figure 4b. g-C_3N_4 6:3 exhibits relative high PL intensity, indicative of rapid

recombination of photogenerated charge carriers. In contrast, a noticeable reduction in PL emission intensity is observed for g-C_3N_4 6:2, demonstrating its superior ability to inhibit electron-hole recombination [23], contributing to the improved degrading efficiency of g-C_3N_4 nanosheets against RhB.

The optical properties of the as-synthesized g-C_3N_4 nanosheets were examined via UV-Vis spectroscopy. Figure 5a reveals the absorption from the ultraviolet region to the visible range with an absorption edge around 400 nm. Furthermore, the optical bandgap energy value (E_g) has been calculated using the Tauc's equation as follows [2]:

$$(\alpha h\nu)^2 = A(h\nu - E_g) \quad (4)$$

where α, ν, A, and E_g are the absorption coefficient, frequency of light, proportionality constant, and energy bandgap. The Tauc plot $(\alpha h\nu)^2$ versus hν exhibits a bandgap of 2.6 eV, indicating a direct electronic transition (Figure 5b). g-C_3N_4 6:2 shows a noticeable red-shift of the edge to approximately 402.6 nm, with a slightly narrower bandgap of 2.5 eV [13]. The small optical gap enhances the light absorption and photocatalytic activity [24].

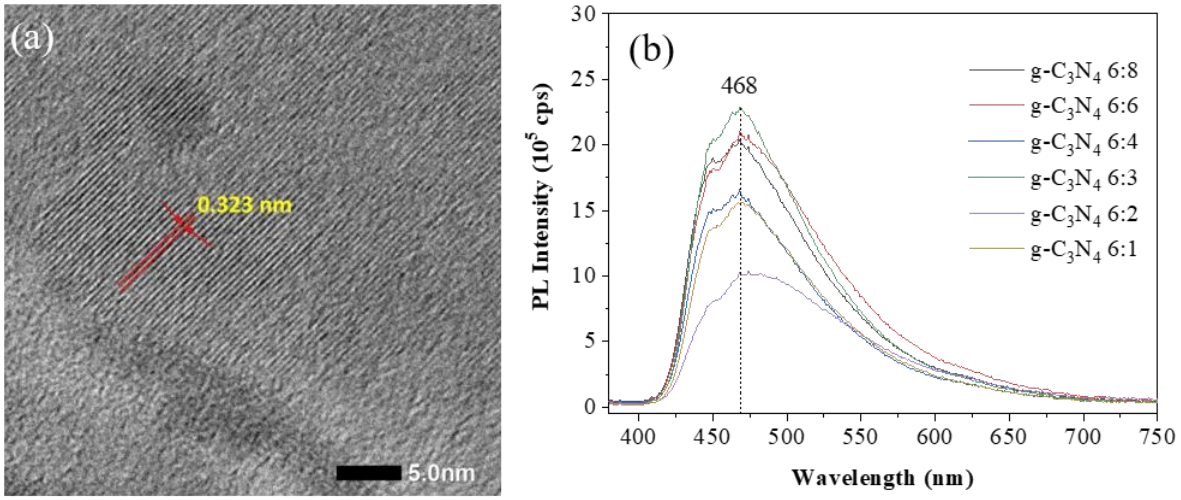

Figure 4. (a) HRTEM image, (b) the photoluminescent spectra of g-C_3N_4 nanosheets.

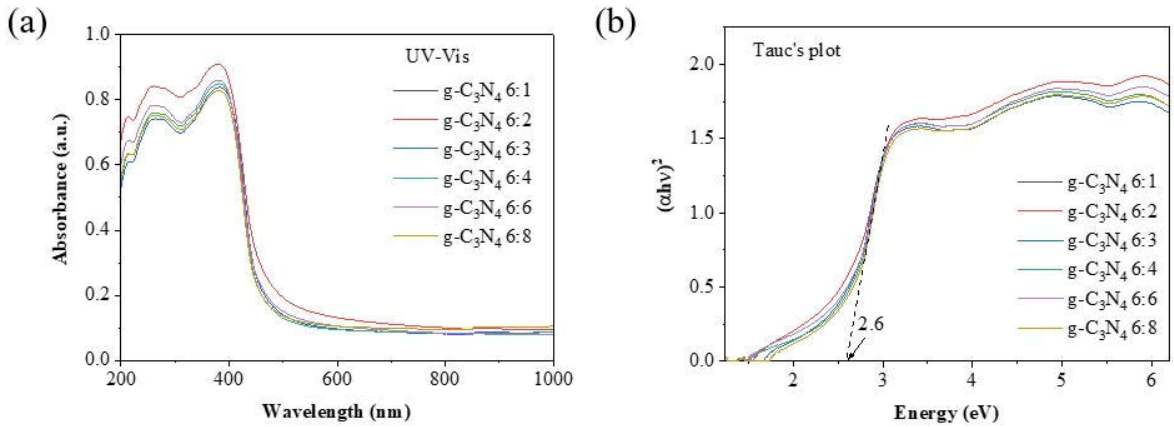

Figure 5. (a) UV-Vis spectrum, (b) Tauc's plot of g-C_3N_4 nanosheets.

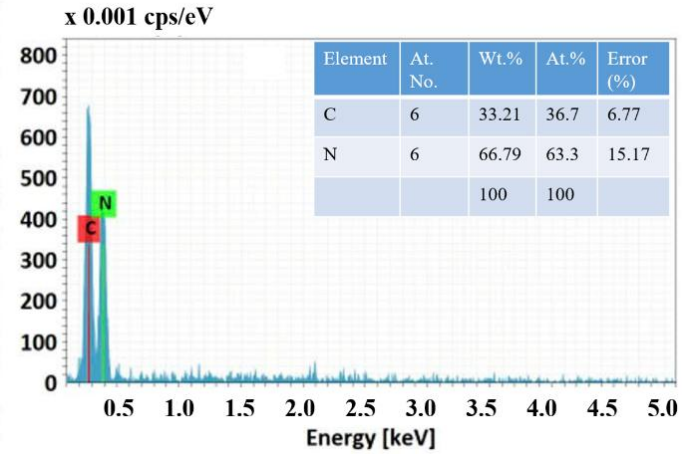

Figure 6. EDS spectrum of g-C_3N_4 6:6 sample.

EDS was employed to obtain the elemental composition and corresponding weight percentages of the g-C_3N_4 sample. The analysis result shown in Figure 6 revealed distinct peaks for the C, N elements, indicating the successful preparation of g-C_3N_4 nanosheets. No other elements were detected, further confirming the purity of the obtained sample.

3.2. Photodegradation of Rhodamine B

In this study, the photocatalytic activity of g-C_3N_4 was evaluated using RhB as a model pollutant under UV light irradiation at room temperature. The degradation process was systematically monitored at 10-min intervals using a UV-Vis spectrophotometer until complete degradation was achieved. RhB degradation occurring in the dark can be negligible. The degradation of RhB was analyzed from g-C_3N_4 6:1 to g-C_3N_4 6:8 and compared with pristine RhB. Among them, g-C_3N_4 6:8 has demonstrated superior photocatalytic effect over other g-C_3N_4 samples. The photodegradation of RhB was completed in 60 min under UV light in the presence of g-C_3N_4 as a photocatalyst.

The photocatalytic reaction of RhB was efficiently achieved using g-C_3N_4 nanosheets as a photocatalyst. As illustrated in Figure 7a, RhB exhibits an absorption peak at 553 nm. The photodegradation efficiency of RhB alone by UV light without a photocatalyst was minimal (59.35%) after 60 min. Without g-C_3N_4 photocatalyst, the photodegradation process was relatively slow with the rate constant (k) of about 0.015 min^{-1} (Figure 7d). Further, the effect of melamine/NH_4Cl ratio on the photodegradation performance of RhB was evaluated using various g-C_3N_4 samples. As shown in Figure 7b, increasing the melamine/NH_4Cl ratio from 6:1 to 6:8 enhanced the photodegradation efficiency and rate.

Table 2. The degradation efficiencies and rate constants of RhB using g-C_3N_4

Sample	Efficiency (%) after 60 min UV light	Rate constant (k, min^{-1})
g-C_3N_4 6:1	99.29	0.086
g-C_3N_4 6:2	99.54	0.096
g-C_3N_4 6:3	99.35	0.090
g-C_3N_4 6:4	99.44	0.097
g-C_3N_4 6:6	98.98	0.084
g-C_3N_4 6:8	99.78	0.114

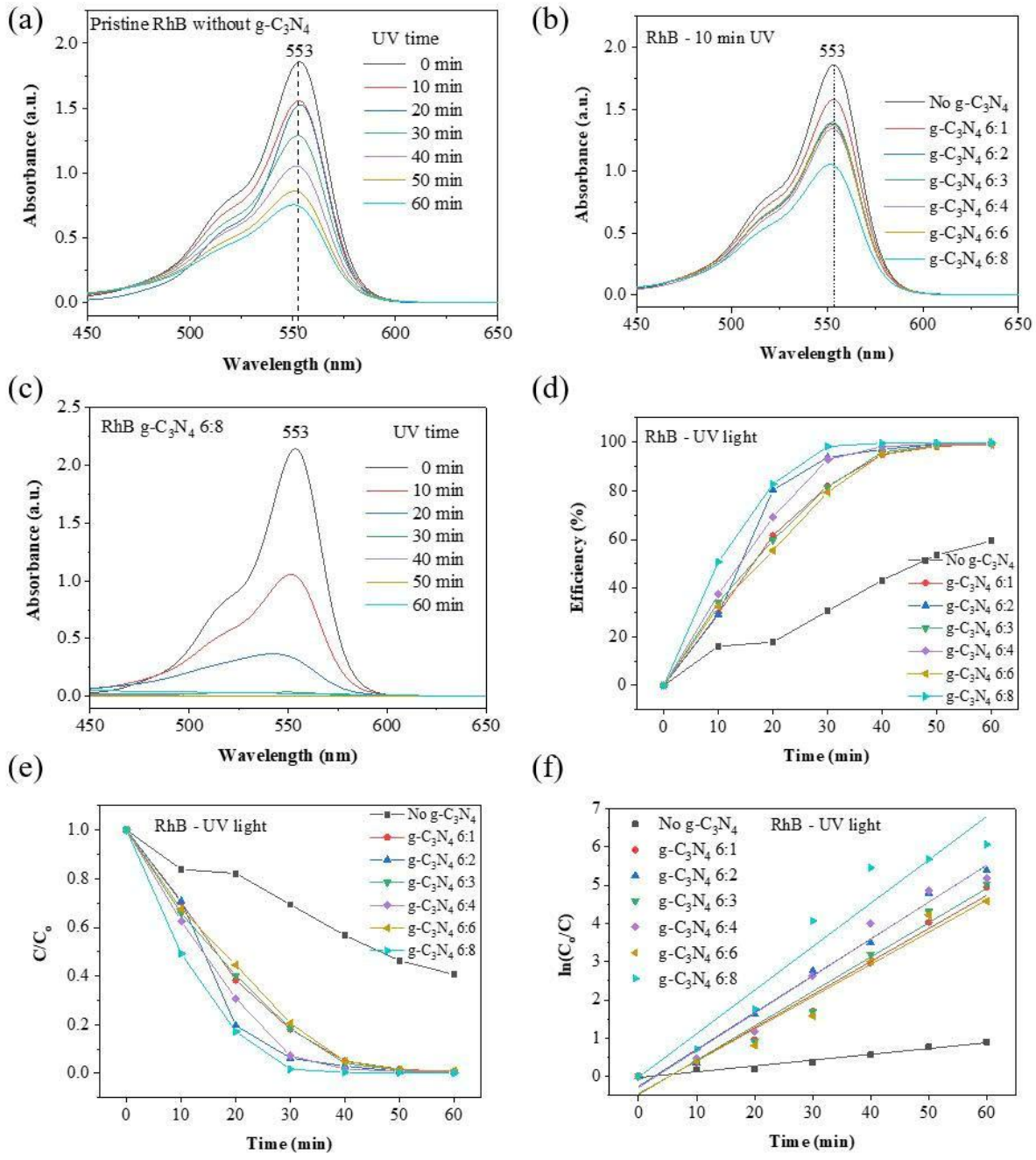

Figure 7. (a) Photocatalytic degradation profile of pristine RhB without g-C_3N_4 under UV illumination, (b) comparison the photocatalytic efficiency of RhB after 10 min UV irradiation using different g-C_3N_4 samples, (c) The absorption spectra of photocatalytic degradation RhB using g-C_3N_4 6:8 as photocatalyst, (d) photodegradation efficiency of RhB using different g-C_3N_4 samples, (e) the change of relative RhB concentration (C/C_o) against UV illumination time using g-C_3N_4 prepared from different melamine/NH_4Cl ratios, (f) the rate constant from the first-order kinetic curve $\ln(C_o/C)$ against time.

In contrast, in the presence of any g-C_3N_4 sample, the photodegradation performance was significantly enhanced with the photodegradation efficiency of approximately 100% achieved within 60 min (Figure 7d), indicating that UV light alone is insufficient for effective photodegradation of RhB and highlighting the essential role of g-C_3N_4 as the photocatalyst. Upon UV illumination, g-C_3N_4 demonstrates markedly superior photocatalytic degradation of RhB compared to bare RhB. g-C_3N_4 showed an enhancement of about 1.68 folds over bare RhB, confirming that g-C_3N_4 significantly improved photocatalytic activity. The application of g-C_3N_4 6:1 photocatalyst resulted in 99.29% degradation, which rose to 99.54% with g-C_3N_4 6:2. The peak degradation of RhB, recorded at 99.78%, was achieved using g-C_3N_4 6:8, as illustrated in Table 2.

Figure 7e depicts the change in relative concentration (C/C_o) over time and Figure 7f presents the pseudo-first-order rate constant (k) for RhB degradation obtained from $\ln(C_o/C)$ against time linear plot. The values of k increased from 0.086 to 0.114 min^{-1} with increasing melamine/NH_4Cl ratio from 6:1 to 6:8, demonstrating a strong dependence of the reaction rate on the g-C_3N_4 sample. The degradation rates of 0.096 and 0.097 min^{-1} were recorded with photocatalysts of g-C_3N_4 6:2 and g-C_3N_4 6:6, respectively.

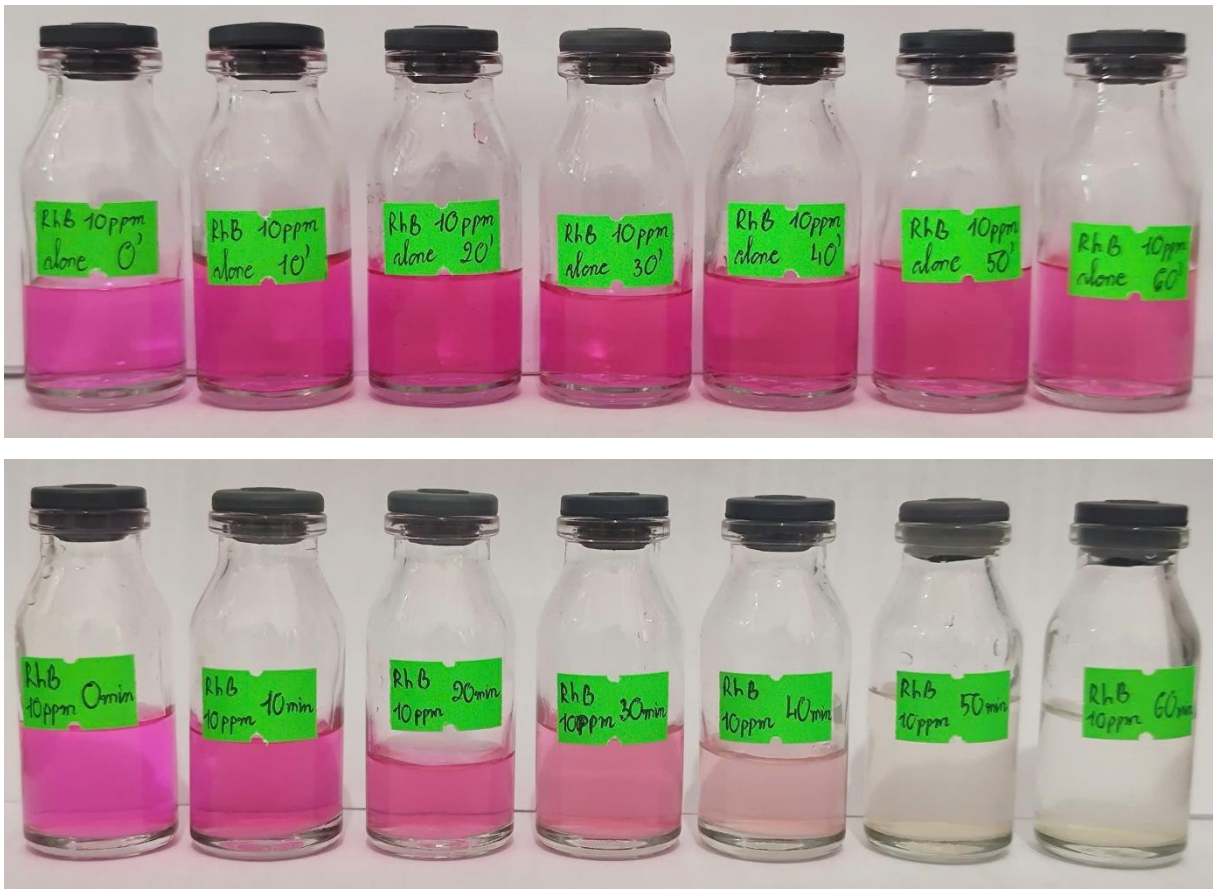

Figure 8. The colour of RhB solution changed under UV light irradiation in the absence (upper image), presence (lower image) of g-C_3N_4 nanosheets.

The highest degradation rate, recorded at 0.114 min^{-1}, was achieved employing g-C_3N_4 6:8 photocatalyst with a rapid photodegradation (~ 50.7% within 10 min of UV illumination) (Figure 7b).

Hence, g-C_3N_4 6:8 was an optimal sample in improving photocatalytic activity. These results suggest that the g-C_3N_4 nanosheets exhibit effective photocatalytic activity in RhB degradation.

Table 3. Comparative photocatalytic performance of pristine g-C_3N_4 and conventional materials for RhB degradation

Materials	Light source	Efficiency (%)	Time (min)	Rate constant (min^{-1})	Ref.
Activated carbon/g-C_3N_4	Visible	95.67	60	0.053	[7]
Spinel oxides	Visible	85.20	60	0.075	[25]
$Ag_3PO_4/CoFe_2O_4$/RGO	Visible	98.65	120	0.029	[23]
TiO_2/Bi_2S_3	Visible	93.80	120	0.021	[26]
Fe_3/Ni_1-g-C_3N_4	Visible	99.20	120	0.045	[27]
g-C_3N_4	UV	99.78	60	0.114	This work

The addition of g-C_3N_4 nanosheets led to a change in the solution colour from pink to colourless demonstrating the degradation of RhB under UV light (Figure 8), followed by a blue shift in the absorption peak to 543 nm (Figure 7c). Superior photocatalytic degradation efficacy for RhB dye underscores the significant impact of this research on the field of environmental science.

To benchmark the photocatalytic performance of g-C_3N_4 nanosheets, a comparative analysis was conducted against previously reported photocatalysts in degrading RhB (Table 3). Pristine g-C_3N_4 nanosheets in this work exhibited the highest efficiency and rate constant within 60 min compared to other photocatalysts. This performance is attributed to the chosen light source and its narrow bandgap. The integration of kinetic modeling, mechanistic insight, and comparative benchmarking highlights the potential of g-C_3N_4 nanosheets for next-generation photocatalysts in environmental remediation.

3.3. Degradation Mechanism

The plausible mechanism for the photocatalyst in the degradation of RhB has been understood as follows. The superior activity of g-C_3N_4 nanosheets was attributed to their enhanced electron transfer across the catalyst surface and adsorption capability, making them a highly efficient and promising photocatalyst for the degradation of RhB dye. The improvement stems from large surface area and rich redox-active sites that promote the dye adsorption and graphitic-mediated reactive oxygen species (ROS) generation. The photocatalytic process of RhB follows pseudo-first-order reaction kinetics in the presence of g-C_3N_4 nanosheets, including four stages [28]: i) Adsorption of RhB molecules on the surface of g-C_3N_4 nanosheets; ii) Diffusion of RhB molecules to the catalyst's active sites; iii) Conversion of RhB to CO_2 and H_2O on the catalyst's surface; iv) desorption of products from the surface. The photogenerated electrons and holes promote the in-situ formation of superoxide radicals ($\cdot O_2^-$) and hydroxyl radicals ($\cdot OH$) [29].

The g-C_3N_4 photocatalysis activity can be described by considering the electronic band structure. The redox mechanism can be deduced from the conduction band (CB) and valence band (CB) potential calculations. The band-edge potential and bandgap of g-C_3N_4 are 4.73 eV and 2.78 eV, respectively [2]. The valence band (VB) and conduction band (CB) positions of g-C_3N_4 were calculated to be 1.62 eV and – 1.16 eV, respectively [15]. Under UV light irradiation, g-C_3N_4 nanosheets absorb photons that possess energy larger than bandgap of g-C_3N_4 ($h\nu > E_g$), promoting electrons from the VB to the CB and leaving holes behind in the VB, generating electron-hole pairs:

$$g-C_3N_4 + h\nu \rightarrow e^-_{CB} + h^+_{VB} \quad (5)$$

The recombination process between electrons in the CB with holes in the VB of g-C_3N_4 removes the weaker reducing electrons and weaker oxidizing holes, leaving strong electrons in the CB and strong holes in the VB of g-C3N4, facilitating the spatial separation of photogenerated electrons and holes. The strongly reducing electrons efficiently convert dissolved O_2 into superoxide radicals ($\cdot O_2^-$), while the highly oxidative holes readily oxidize water to hydroxyl radicals ($\cdot OH$) and H^+ ions [14].

$$e^-_{CB} + O_2 \rightarrow \cdot O_2^- \quad (6)$$

$$h^+_{VB} + H_2O \rightarrow \cdot OH + H^+ \quad (7)$$

The low positive valence band potential of g-C_3N_4 (1.62 eV) indicates that the holes on the valence band are unable to produce $\cdot OH$ through a reaction with hydroxide ions (OH^-) [30]. Additionally, the conduction band electrons of g-C_3N_4 possess a more negative potential of -1.22 eV and are capable of initiating the reduction of adsorbed O_2 molecules to $\cdot O_2^-$. $\cdot O_2^-$ radicals can undergo protonation with H^+ ions to form hydroxyl radicals ($\cdot OH$) [31].

$$\cdot O_2^- + 2H^+ \rightarrow 2 \cdot OH \quad (8)$$

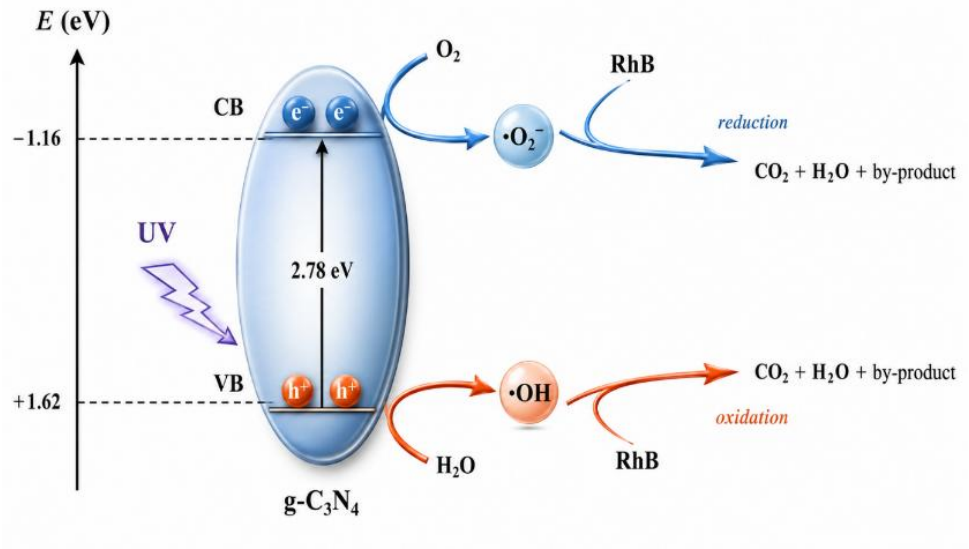

Figure 9. Plausible mechanism for photocatalytic degradation of RhB using g-C_3N_4 nanosheets.

These reactive oxygen species ($\cdot O_2^-$ and $\cdot OH$) attack and decompose RhB molecules into CO_2, H_2O, and other mineralized products until complete mineralization (Figure 9).

$$146 \cdot OH + C_{28}H_{31}ClN_2O_3 \rightarrow 28CO_2 + 87H_2O + HCl + 2HNO_3 \quad (9)$$

$$65 \cdot O_2^- + 2C_{28}H_{31}ClN_2O_3 \rightarrow 56CO_2 + 24H_2O + 2NH_3 + 2NH_4Cl + 65e^- \quad (10)$$

The previous experiments specified the h^+ and $\cdot O_2^-$ significant involvement of dye degradation and the moderate role of electrons and $\cdot OH$. It is said that g-C_3N_4 strengthens redox capability and significantly accelerates the photocatalytic degradation of RhB. g-C_3N_4 demonstrated excellent photocatalyst for the removal of organic pollutants from water resources.

An increase in melamine/NH_4Cl weight ratio from 6:1 to 6:8 results in a greater generation of hydroxyl free radical due to an augmentation of active sites on the catalyst's surface, enhancing the effectiveness of photocatalytic degradation. The photocatalytic process is influenced by the shape, size, active surface area of the photocatalyst, and light source. The high rate is attributed to the use of ultraviolet light instead of visible radiation.

4. Conclusions

In summary, g-C_3N_4 nanosheets were successfully synthesized via a thermal polymerization approach and demonstrated excellent photocatalytic performance for the removal of Rhodamine B (RhB). XRD, TEM, HRTEM, UV-Vis, PL, and EDS techniques revealed the crystalline phase, sheet-like morphology, size, lattice spacing, and bandgap of g-C_3N_4. The obtained product efficiently photodegraded RhB with 99.78% efficiency within 60 min ($k = 0.114\ min^{-1}$) under UV light (365 nm). The high activity of g-C_3N_4 nanosheets arises from abundant active sites on their surfaces for RhB adsorption, redox-active centers and electron transfer. UV photons generate superoxide and hydroxyl radicals that are the effective agents for photodegrading RhB molecules. Overall, g-C_3N_4 nanosheets are efficient catalyst for the sustainable removal of organic pollutants from aqueous systems.

Acknowledgement

The authors sincerely acknowledge the financial support provided by Vietnam National Foundation for Science and Technology Development (NAFOSTED) under grant number NCUD.01-2025.23.

References

[1] V. Saxena, Water Quality, Air Pollution, and Climate Change: Investigating the Environmental Impacts of Industrialization and Urbanization, Water, Air, Soil Pollut., Vol. 236, 2025, pp. 73, https://doi.org/10.1007/s11270-024-07702-4.

[2] K. Upendranath, P. Mukherjee, G. V. Megha, K. Manjunath, R. S. Vishwanath, M. Mahanthappa, M. D. Kurkuri, A Multifunctional FeS_2/S–g–C_3N_4 composite for Catalytic Reduction of 4-Nitrophenol and Photocatalytic Degradation of Methylene Blue Dye, Appl. Surf. Sci., Vol. 735, 2026, pp. 166681, https://doi.org/10.1016/j.apsusc.2026.166681.

[3] M. Kumar, V. P. Singh, S. B. Bhat, R. Kumar, Environmental Risks of Textile Dyes and Photocatalytic Materials for Sustainable Treatment: Current Status and Future Directions, Discov. Environ., Vol. 3, 2025, pp. 132, https://doi.org/10.1007/s44274-025-00337-0.

[4] R. H. Waghchaure, V. A. Adole, B. S. Jagdale, Photocatalytic Degradation of Methylene Blue, Rhodamine B, Methyl Orange and Eriochrome Black T Dyes by Modified ZnO Nanocatalysts: A Concise Review, Inorg. Chem. Commun., Vol. 143, 2022, pp. 109764, https://doi.org/10.1016/j.inoche.2022.109764.

[5] B. Liu, Y. Tian, Z. Liu, L. Yi, F. Li, Y.-H. Liu, X. Huang, Innovative Construction of Sulfur-Self-Doped g-C_3N_4/$CuFeO_2$ S-Scheme Heterojunction for Photocatalytic Removal of Rhodamine B: Mechanism and Detoxification Assessment, J. Photochem. Photobiol. A: Chem., Vol. 479, 2026, pp. 117231, https://doi.org/10.1016/j.jphotochem.2026.117231.

[6] P. Molaei, F. R. Moghadam, Rapid Thermal Shock Synthesis of Se/g-C_3N_4 S-Scheme Heterojunctions for Enhanced Photocatalytic Applications, Ceram. Int., Vol. 52, 2026, 17149-17159, https://doi.org/10.1016/j.ceramint.2026.02.301.

[7] L. N. Thi, T. T. T. Phan, L. N. Tan, T. L. T. Le, L. T. Nguyen, N. T. Hoang, V. Vo, D. Q. Khieu, Activated Carbon/gC_3N_4/H_2O_2 System with Enhanced Photocatalytic Activity for Rhodamine-B Degradation under the Visible Light, Environ. Eng. Res., Vol. 30, 2025, pp. 240121, https://doi.org/10.4491/eer.2024.121.

[8] S. Almotiry, A. A. Algreiby, G. S. Alrebdi, F. M. Al Suqayhi, N. G. Sabeel Al Harbi, M. A. Ibrahem, M. A. B. Aissa, Boosting the Photocatalytic Ability of BaZnO by g-C_3N_4 for Anionic and Cationic Dyes Degradation, Diam. Relat. Mater., Vol. 165, 2026, pp. 113655, https://doi.org/10.1016/j.diamond.2026.113655.

[9] H. Q. Luu, M. T. Pham, Y. F. Wang, S. J. You, Enhancing NO Degradation in Visible Light through Plasma-Treated Photocatalytic Substrates Featuring TiO_2@g-C_3N_4 Z-Scheme Structure, Environ. Eng. Res., Vol. 29, 2024, pp. 230560, https://doi.org/10.4491/eer.2023.560.

[10] C. Chu, Q. Zhu, Z. Pan, S. Gupta, D. Huang, Y. Du, S. Weon, Y. Wu, C. Muhich, E. Stavitski, Spatially Separating Redox Centers on 2D Carbon Nitride with Cobalt Single Atom for Photocatalytic H_2O_2 Production, PNAS, Vol. 117, 2020, pp. 6376-6382, https://doi.org//10.1073/pnas.1913403117.

[11] Q. Zhu, Y. Shi, Y. Tao, L. Fu, C. Zhang, H. Shang, D. Zhang, G. Li, Binary Heteroatom Dopants Enable Carbon-Based Heterostructures for Efficient Photoelectrocatalytic H_2O_2 Synthesis in a Wide pH Range, Chem. Eng. J., Vol. 482, 2024, pp. 149066, https://doi.org/10.1016/j.cej.2024.149066.

[12] Y. Wang, F. Liang, Z. Chen, Piezoelectric Polarization Field Modulation of the Schottky Barrier in Pt/g-C_3N_4 Heterojunctions: Enhanced Photocatalytic Activity via Hot Electron Transfer, J. Environ. Chem. Eng., Vol. 14, 2026, pp. 122175, https://doi.org/10.1016/j.jece.2026.122175.

[13] M. Yaqoubi, M. Salavati-Niasari, M. Ghanbari, S-Scheme $CuMn_2O_4$/g-C_3N_4 Heterojunction: Fabrication, Characterization, and Investigation of Photodegradation Potential of Organic Pollutants, Appl. Water. Sci., Vol. 15, 2025, pp. 13, https://doi.org/10.1007/s13201-024-02348-3.

[14] M. Niknam, M. B. Vandchali, E. Ghasemi, A. Kazemi, N. Yousefi-Limaee, Synthesis and Characterization of a Novel g-C_3N_4/NiAl-LDH/CeO_2 Photocatalyst for Degradation of Rhodamine B, Int. J. Environ. Sci. Technol., Vol. 22, 2025, pp. 4215-4228, https://doi.org/10.1007/s13762-024-06052-2.

[15] O. V. Alekseeva, V. D. Shibaeva, A. V. Noskov, A. V. Agafonov, Synthesis and Photocatalytic Activity of the TiO_2/g-C_3N_4 Composites: Influence of the TiO_2 Particles Morphology (Rod or Spherical) on Degradation of Organic Dyes, Phys. B: Condens. Matter, Vol. 727, 2026, pp. 418302, https://doi.org/10.1016/j.physb.2026.418302.

[16] S. H. Ammar, A. I. Alyibe, H. J. Hadi, Constructing ZIF-67 over S-Doped g-C_3N_4 Composites with Enhanced Photocatalytic Degradation Performance toward Organic Pollutants, J. Photochem. Photobiol., Vol. 33, 2026, pp. 100283, https://doi.org/10.1016/j.jpap.2026.100283.

[17] M. Khairy, M. A. B. Aissa, A. Modwi, E. M. Masoud, N. Raza, Optimizing Aquatic Cleanup of Ciprofloxacin by Means of RuO_2-Co_3O_4@g-C_3N_4 Nanocomposite, Diam. Relat. Mater., Vol. 155, 2025, pp. 112268, https://doi.org/10.1016/j.diamond.2025.112268.

[18] M. Mahanthappa, M. P. Bhat, A. Alshoaibi, Exploring the Role of Redox-Active Species on NiS-NiS2 Incorporated Sulfur-Doped Graphitic Carbon Nitride Nanohybrid as a Bifunctional Electrocatalyst for Overall Water Splitting, Int. J. Hydrog. Energy, Vol. 84, 2024, pp. 641-649, https://doi.org/10.1016/j.ijhydene.2024.08.220.

[19] H. Khiar, L. C. Valencia-Valero, N. Barka, A. Puga, (Ag–NiO)/g-C_3N_4 with Enhanced Photocatalytic Activity for Hydrogen Evolution under Simulated Sunlight, Int. J. Hydrog. Energy, Vol. 91, 2024, pp. 39-49, https://doi.org/10.1016/j.ijhydene.2024.09.377.

[20] F. Saman, C. H. S. Ling, A. Ayub, N. H. B. Rafeny, A. H. Mahadi, R. Subagyo, R. E. Nugraha, D. Prasetyoko, H. Bahruji, Review on Synthesis and Modification of g-C_3N_4 for Photocatalytic H_2 Production, Int. J. Hydrog. Energy, Vol. 77, 2024, pp. 1090-1116, https://doi.org/10.1016/j.ijhydene.2024.06.212.

[21] A. V. Zhurenok, P. A. Tkachenko, A. E. Ermoshkina, D. D. Mishchenko, E. E. Aydakov, E. Y. Gerasimov, E. A. Kozlova, Effect of Ni Loading on the Structure and Photocatalytic Performance of g-C_3N_4-Based Photocatalysts, Inorg. Chem. Commun., Vol. 188, 2026, pp. 116505, https://doi.org/10.1016/j.inoche.2026.116505.

[22] C. Prasad, K. Sreenivasulu, S. Gangadhara, P. Venkateswarlu, Bio Inspired Green Synthesis of Ni/Fe_3O_4 Magnetic Nanoparticles Using Moringa Oleifera Leaves Extract: A Magnetically Recoverable Catalyst for Organic Dye Degradation in Aqueous Solution, J. Alloys Compd., Vol. 700, 2017, pp. 252-258, http://dx.doi.org/10.1016/j.jallcom.2016.12.363.

[23] M. Kaur, A. Kumar, S. M. Siddeeg, M. Selvaraj, S. Gautam, Dual-Functional Ag_3PO_4/$CoFe_2O_4$/RGO Nanocomposite for Visible-Light-Driven Photocatalytic Degradation of Rhodamine B and Tramadol and Antibacterial Applications, Surf. Interfaces, Vol. 90, 2026, pp. 109194, https://doi.org/10.1016/j.surfin.2026.109194.

[24] G. H. Shahverdizadeh, K. Seyyedi, A. Mehrizad, R. Majdan-Cegincara, S. Jamshidi, E. Ghasemi, P. Gharbani, M. Farbodi, M. Es' hagi, Recent Insights into g-C_3N_4 Based Composites for Methylene Blue Photocatalytic Degradation, Results Eng., Vol. 29, 2025, pp. 108595, https://doi.org/10.1016/j.rineng.2025.108595.

[25] I. Bencherifa, K. Derkaoui, A. Elfiad, M. Trari, B-Site Engineered High-Entropy Spinel Oxides for Efficient Visible-Light Photocatalytic Degradation of Rhodamine B, J. Phys. Chem. Solids, Vol. 213, 2026, pp. 113588, https://doi.org/10.1016/j.jpcs.2026.113588.

[26] X. Zeng, X. Wang, Y. Zhai, Y. Wang, Enhanced Photocatalytic Degradation of Rhodamine B by a Novel MT-TiO_2/Bi_2S_3 Composite under Simulated Solar Light, Mater. Sci. Semicond. Process., Vol. 211, 2026, pp. 110721, https://doi.org/10.1016/j.mssp.2026.110721.

[27] I. T. Mwizerwa, J. Tang, T. Huang, L. Zelong, Z. Sun, X. Zhao, Enhanced Photocatalytic Degradation of Rhodamine B via Iron/Nickel Co-Doped Graphitic Carbon Nitride: Synthesis, Degradation Mechanism, and DFT Insights, Polyhedron, Vol. 290, 2026, pp. 118040, https://doi.org/10.1016/j.poly.2026.118040.

[28] S. Samadder, A. Pandit, M. F. Ahmed, B. Biswas, U. S. Akhtar, T. Paul, M. K. Hossain, N. Sharmin, M. S. Islam, M. E. Halim, Tailoring the Structure and Morphology of Hematite via Zn Doping for Superior Photocatalytic Degradation of Rhodamine B, Open Ceram., Vol. 26, 2026, pp. 100943, https://doi.org/10.1016/j.oceram.2026.100943.

[29] H. Fazlı, Z. Biyiklioglu, Ö. Kesmez, F. Demir, Synthesis of Water-Soluble Phthalocyanine-Modified Nano TiO_2 functional Thin Films and Investigation of Their Photocatalytic Activities against Methylene Blue and Rhodamine B Pollutants, Inorg. Chem. Commun., Vol. 189, 2026, pp. 116653, https://doi.org/10.1016/j.inoche.2026.116653.

[30] J. Yu, S. Wang, J. Low, W. Xiao, Enhanced Photocatalytic Performance of Direct Z-scheme g-C_3N_4–TiO_2 Photocatalysts for the Decomposition of Formaldehyde in Air, Phys. Chem. Chem. Phys., Vol. 15, 2013, pp. 16883-16890, https://doi.org/10.1039/C3CP53131G.

[31] H. Li, S. Gan, H. Wang, D. Han, L. Niu, Intercorrelated Superhybrid of AgBr Supported on Graphitic-C_3N_4-Decorated Nitrogen-Doped Graphene: High Engineering Photocatalytic Activities for Water Purification and CO_2 Reduction, Adv. Mater., Vol. 27, 2015, pp. 6906-6913, https://doi.org/10.1002/adma.201502755.